Poly(ester)s and Poly(amide)s with Fluorene and Diphenyl-Silane Units in the Main Chain: Effects of Iodine Doping on the Structure and Electrical Conductivity

Carmen M. González Henríquez,[1] Luis H. Tagle,[1] Claudio A. Terraza,[1] Andrés Barriga González,[2] A. L. Cabrera,[3] Ulrich G. Volkmann[3]

[1]*Departamento de Química Orgánica, Facultad de Química, Pontificia Universidad Católica de Chile, P.O. Box 306, Santiago 6094411, Chile*
[2]*Departamento de Bioquímica y Biología Molecular, Facultad de Ciencias Químicas y Farmacéuticas, Universidad de Chile*
[3]*Facultad de Física, Pontificia Universidad Católica de Chile, P.O. Box 306, Santiago 6094411, Chile*

Received 7 December 2010; accepted 18 August 2011
DOI 10.1002/app.35499
Published online 22 December 2011 in Wiley Online Library (wileyonlinelibrary.com).

ABSTRACT: Intramolecular charge transfer interaction between the electron donor and electro acceptor units within the polymeric structure and its optoelectronic properties were studied. The monomer, 9*H*-fluorene-2,7-dicarboxylic acid, was prepared from 9*H*-fluorene-2,7-dicarbonitrile using CuCN/*N*,*N*-dimethylformamide followed by the decomposition of the complex with $FeCl_3x6H_2O$ in HCl and KOH/H_2O. The formation of two new classes of polymers was reported at different reaction times. The poly(ester) (PEF) was synthesized by the reaction of the diacid monomer with bis(4-hydroxiphenyl)diphenylsilane using tosyl chloride/pyridine/dimethylformamide system as condensing agent. Alternatively, the poly(amide) (PAF) was synthesized by the direct polycondensation of the diacid monomer and bis(4-aminophenyl)diphenylsilane in *N*-methyl-2-pyrrolidine solution containing dissolved calcium chloride. The resulting new polymers were obtained in good yields and were characterized by FTIR, NMR (^1H, ^{13}C, and ^{29}Si), ESI, Raman, UV (optical gap) and fluorescence spectroscopy. The thermal properties were characterized by DSC and TGA. The electrical conductivity of the polymers was measured before and after exposure to iodine vapor, utilizing films of different thickness. Ellipsometric studies were used for the determination of the film thickness. Morphological differentiation was carried out by SEM-EDX analysis. Oxidation of the polymer films of low thickness decreased their conductivities, mainly due to the small structural changes. For a polymeric sample with a higher thickness, the doping process slightly increased the conductivity. © 2011 Wiley Periodicals, Inc. J Appl Polym Sci 125: 477–487, 2012

Key words: charge transfer; conducting polymers; film; mass spectrometry; Raman spectroscopy

INTRODUCTION

In the last years σ–conjugated polymers, such as poly(germylene)s and especially poly(silylene)s, have received widespread interest in the research community due to their electrical and optical properties. The poly(silylene)s are very important materials due to their photochemical properties and for this reason they are commonly used in technological applications. Some of these applications are: semiconducting materials, photoreceptors in electrophotography and as part of devices that require nonlinear optical material.[1–9] Their electronic properties are associated with electron conjugation in the silicon atom, which allows a significant delocalization of electrons along of the polymeric chain. Therefore, the incorporation of a silicon atom in the main chain of a polymer increases the solubility due to the reduction of the packing force and the increase of the free volume of the system. In addition, most of the silicon-containing aromatic polymers maintain a high thermal stability as a consequence of the ionic character of the Si-bond; these properties have been widely studied by our research group.[10–18]

On the other hand, the conductivity of polymers is intimately connected to the mobility of charge carriers, which in turn depends on the structure and morphology of the system.[19] At present, it is still very important to understand and improve the process undergoing the molecules from a disordered state in solution into the semiordered solid state (film). This process should be associated with the typical conductivity for doped conjugated polymers and the mobility of charge carriers on the surface of the sample.

Correspondence to: C. M. González Henríquez (cgonzalen@puc.cl).

Contract grant sponsor: FONDECYT; contract grant numbers: 1100015, 1095151, 1100882.
Contract grant sponsor: MECESUP UCH N°0601.
Contract grant sponsor: VRI Puente N° 3/2011.

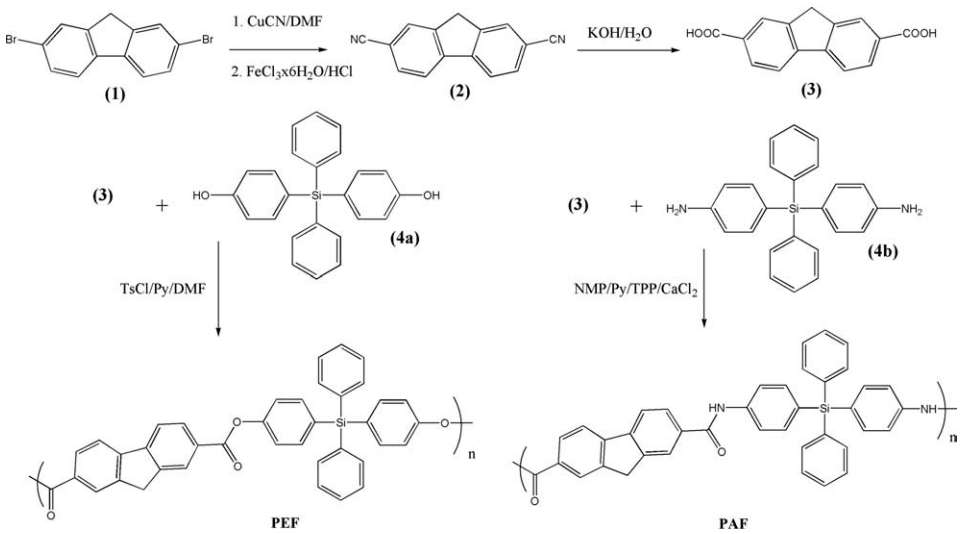

Figure 1 Synthetic route for the preparation of the poly(ester) (PEF) and poly(amide) (PAF).

In this study, we report the synthesis of two kinds of polymers: poly(ester) (PEF) and poly(amide) (PAF) with fluorene and diphenyl-silane units in the main chain (Fig. 1), where the conjugation or resonance is interrupted by the ester and amidic groups. The characterization of the monomers was carried out by FTIR, NMR (^{1}H and ^{13}C) and elemental analysis. Polymers were characterized by the same technique used for the monomers and by additional measurements, described below. The incorporation of Si into of the polymeric structure was followed by ^{29}Si NMR spectroscopy. Effective mass determination of the polymers was obtained by electrospray ionization (ESI) and the vibration frequencies of some functional groups were determined by FTIR and corroborated by Raman spectroscopy. In addition, the structural information was obtained from X-ray characterization. However, one of the major purposes of our investigation is to determine the electrical conductivity of the polymeric film at different thickness, using an oxidative method, such as iodine vapors, and correlate these results with the optical band-gaps obtained by UV-vis analysis, and using Tauc's expression.[20] The structural and surface morphology of films were carried out by scanning electron microscope (SEM-EDX) analysis.

EXPERIMENTAL PART

Materials and equipments

For the synthesis described below, we used the following materials: Hydrate ferric chloride ($FeCl_3x6H_2O$), cuprous cyanide (CuCN), 4-bromophenol, 4-bromo-*N*,*N*-bis(trimethylsilyl)aniline, dichlorodiphenylsilane, *N*-methyl-2-pyrrolidone (NMP), triphenyl phosphite (TPP), pyridine, *N*,*N*-dimethylformamide (DMF), and tosyl chloride (TsCl), all supplied by Sigma-Aldrich.

Anhydrous calcium chloride ($CaCl_2$), lithium and n-butyl bromide, were obtained from Merck (Darmstadt, Germany). Tetrahydrofuran and diethyl ether were dried by distillation over sodium wire.

The samples were analyzed with the following equipments: The infrared spectra were measured on a Perkin-Elmer FTIR-1310 spectrophotometer, using a OPUS 2.0 software. ^{1}H, ^{13}C, and ^{29}Si NMR analyses were recorded on a Bruker 400 MHz spectrometer in DMSO-d_6 and acetone-d_6 as solvent, using tetramethylsilane (TMS) as internal standard. The non modified carbons in ^{135}dept analysis are shown with an asterisk over their chemical shift. Elemental analysis of the monomers was carried out in a Fison EA- 1108 instrument. Absorption spectra of the polymers were recorded with an Agilent 8453 diode array spectrophotometer and the band gap energy (E_g) of the compounds was calculated from their adsorption edges. The spectra were recorded by using DMSO at 25°C. The fluorescence spectra of polymer solution in 10 μL of DMSO or H_2SO_4 and 2.9 mL of acetone were obtained by a Perkin Elmer (Model LS-55) luminescence spectrometer equipped with a 7.3 W/50Hz xenon source.

Effective mass of the polymers was determined by Liquid Chromatography-Mass spectrometry (LC-MS). All experiments were performed on a HPLC Agilent 1100 (Agilent Technologies, CA-USA), which was interfaced to an ESI-IT Esquire 400 (Bruker Daltonik GmbH, Germany). The chromatograms were processed using the ChemStation softwares for LC 3D Rev. A.10.02 (Agilent Technologies, CA-USA) and Esquire-Control 5.2 (Bruker Daltonik, GmbH, Germany). Phenomenex Luna (C18, 150. Ũ 4.6 mm, 5 μm particles, 100 Å pores) was used as column for fragmentation studies. The samples were dissolved in 50 μL of DMSO or H_2SO_4 in 950 μL of acetone. The separation

of 20 μL was realized at room temperature. Drying gas was nitrogen (flow 10.0 L/min, 325°C), and the nebulizer pressure was set to 30 psi or 206842.8 Pa. The spectra were acquired in positive and negative mode.

DSC traces were recorded after the second heating run on a Mettler Toledo DSC 821e differential scanning calorimetric and thermal degradation temperatures in a TGA/SDTA 851e Mettler Toledo termobalance. Both analyses were recorded at a heating rate of 20°C min^{-1} under nitrogen atmosphere.

X-ray diffraction patterns of polymers were taken at room temperature with a Bruker D-8 Advanced Diffractometer, using a tube with a copper anode ($\lambda(CuK\alpha) = 0.154$ nm). The diffraction patterns were obtained in the usual θ–2θ geometry. The X-ray tube was operated at 40 kV and 40 mA. The goniometer was swept between 5° and 140° at 0.02°/s over the whole 2θ interval. The diffracted X-rays were analyzed with a scintillation detector.

The structural and vibrational properties of the polymers were characterized by Raman spectroscopy with a LabRam 010 instrument from ISA using a 5.5 mW, 633 nm He-Ne laser without filter. The integration time for each spectrum was 5 s. The Raman microscope uses a backscattering geometry, where the incident beam is linearly polarized and the spectral detection unpolarized. The objective lens of the microscope was an Olympus Mplan 100x (Numerical aperture 0.9), which provided sufficient distance between the objective and the sample.

The film thickness at room temperature was determined using a single wavelength null ellipsometer in PCSA configuration at 632.8 nm. The angle of incidence of the beam was 60° with respect to the normal sample. From the ellipsometric Δ and Ψ parameters, corresponding to the measured polarizer and analyses angles, the film thickness was determined with a single layer Drude model. The morphology of the film was examined with a scanning electron microscope (SEM), model LEO 1420VP, 100 μA beam current and a working distance of 6 mm. The microscope was operated at high vacuum ($\sim 10^{-6}$ mbar).

Monomer synthesis

9H-fluorene-2,7-dicarbonitrile (2)

A stirred mixture of 2,7-dibromo-9*H*-fluorene (Fig. 1) (**1**) (4.3 g, 13.3 mmol), cuprous cyanide (2.92 g, 32.6 mmol) and DMF (10 mL) was refluxed for 24 h.[21] The resulting brown mixture was poured into a solution of hydrate ferric chloride (10.6 g, 39.1 mmol), and conc. HCl (3.2 mL) in water (16 mL) and maintained at 70°C for 1 h to decompose the complex. After heating, the dark solution was extracted twice with chloroform and the extracts washed with dilute HCl (1 : 1), 10% aqueous sodium hydroxide and water. Subsequently, the solution was dried over anhydrous $MgSO_4$, filtered and the solvent evaporated, obtaining a yellow solid. The total yield of the reaction for the compound was 55%, with a m.p. of 316.3–317.8°C.

IR (KBr, cm^{-1}): 3083, 3059 (C—H arom. stretching), 2945 (C—H aliph. stretching), 2222 (C≡N stretching), 1465 (C—H aliph. bending), 1614, 1577, 1404 (C=C arom. stretching), 821 (C—H arom. "out of plane" (*oop*) bending). ^{1}H NMR (Acetone-d_6): 8.22 (d, 2H, *J*= 8.0 Hz), 8.07 (s, 2H), 7.87 (d, 2H, *J*= 7.9 Hz), 4.18 ppm (s, 2H). ^{13}C NMR (Acetone-d_6): 146.1, 145.1, 132.3*, 130.1*, 123.0*, 119.7, 112.3, 37.5* ppm. Elem. Anal. Calcd. for $C_{15}H_8N_2$; (216.24): C, 83.32%; H, 3.73%; N, 12.95%. Found: C, 81.16%; H, 4.58%; N, 12.60%.

9H-fluorene-2,7-dicarboxylic acid (3)

In a 250-mL flask, a suspension of 9*H*-fluorene-2,7-dicarbonitrile (**2**) (Fig. 1) (2.52 g, 11.7 mmol) in 140 mL of an ethanol/water mixture (1 : 1) solution containing (13.1 g, 234 mmol) of KOH was refluxed for about one week until the evolution of ammonia had ceased. The hot solution was allowed to cool and acidified by conc. HCl to pH 2–3. The black solid thus obtained was collected by filtration, washed with water, petroleum ether, and dried in vacuum at 60°C to afford 71% of the diacid **3**, with a m.p. of 338.1–339.6°C.

IR (KBr, cm^{-1}): 3413-2543 (O—H stretching), 2943 (C—H aliph. stretching), 1684 (C=O stretching), 1413 (CH aliph. bending), 1609, 1583, 1473 (C=C arom. stretching), 760 (C—H arom. *oop* bending). ^{1}H-NMR (DMSO-d_6): 13.03 (s, 2H), 8.18 (s, 2H), 8.09 (d, *J*= 8.1 Hz, 2H), 8.02 (d, *J*= 8.2 Hz, 2H), 4.08 ppm (s, 2H). ^{13}C-NMR (DMSO-d_6): 167.4, 144.3, 144.2, 129.9*, 128.4, 126.2*, 120.8*, 36.4* ppm. Elem. Anal. Calcd. for $C_{15}H_{10}O_4$; (254.24): C, 70.86%; H, 3.96%; O, 25.17%. Found: C, 69.70%; H, 3.92%; O, 26.38 %.

The bisphenol (**4a**) and the diamine (**4b**) were prepared according to a procedure described in the literature.[22–24]

Polymer synthesis

The polymers are designated as PEF-2, PEF-12, PAF-3, and PAF-12, according with the hours of polymerization.

The poly(ester)s (Fig. 1) were prepared by the following procedure[25–27]: A pyridine (0.6 mL, 7.43 mmol) solution of TsCl (0.64 g, 3.35 mmol) was treated with DMF (0.2 mL, 2.58 mmol) for 30 min and the resulting solution was added dropwise to a solution of diacid (**3**) (0.57 g, 1.56 mmol) in pyridine (0.6 mL), which was maintained at room temperature for 30 min. To this mixture, a solution of the

bisphenol (**4a**) (0.39 g, 1.56 mmol) in pyridine (0.6 mL) was added dropwise and the whole solution was stirred at room temperature for 20 min and then at 120°C for 2 h. The viscous liquid was precipitated in 100 mL of methanol with stirring. The yellow precipitate was collected by filtration, washed with methanol and dried. The yields of the polymer were: PEF-2 (71%) and PEF-12 (82%).

The poly(ester)s (PEF-2 and PEF-12) had the same spectra, as follows: IR (KBr, cm^{-1}): 3070, 3023 (C—H arom. stretching), 2941 (C—H aliph. stretching), 1686, 1014 (C=O stretching), 1611 (Si—C arom.), 1587 (C—C arom. stretching), 1429 (C—H aliph. bending), 699 (C—H arom. *oop* bending). ^{1}H-NMR (DMSO-d_6): 8.16 (s, 2H), 8.07-8.01 (dd, 2H), 7.55-7.53 (dd, 2H), 7.46-7.20 (m, 18H), 4.06 ppm (s, 2H). ^{13}C-NMR (DMSO-d_6): 167.8, 144.8, 136.5, 134.4, 134.1, 131.4*, 130.9, 130.4*, 130.1*, 128.9, 128.6*, 128.3*, 128.0*, 126.7*, 121.3*, 36.9* ppm. ^{29}Si-NMR (DMSO-d_6): −15.4 ppm. Elem. Anal. Calcd. for $C_{39}H_{26}O_4Si$; (586.48): C: 79.86%; H: 4.43%. Found: C: 78.82%; H: 3.37%.

The Poly(amide)s (Fig. 1) were prepared by the following procedure[28]: A mixture of 9*H*-fluorene-2,7-dicarboxylic acid (**3**) (0.23 g, 0.90 mmol), bis(4-aminophenyl)diphenylsilane (**4b**) (0.33 g, 0.90 mmol), calcium chloride (0.22 g), TPP (0.65 mL), pyridine (0.57 mL) and NMP (1.1 mL) was heated with stirring at 110°C for 3 h. The reaction mixture was trickled into 100 mL of methanol with stirring, giving a light brown precipitate that was washed thoroughly with methanol and dried. The yields of the polymers were: PAF-3 (80%) and PAF-12 (85%).

The same (^{1}H, ^{13}C, ^{135}dept, and ^{29}Si) NMR spectra for the polymers PAF-3 and PAF-12 were obtained, as follows: IR (KBr, cm^{-1}): 3417 (N—H stretching), 3077-2927 (C—H arom. stretching), 2244 (C—H aliph. stretching). 1656 (C=O stretching), 1586 (Si—C arom.), 1509 (C=C arom. stretching), 1429 (C—H aliph. bending), 700 (C—H arom. *oop* bending). ^{1}H-NMR (DMSO-d_6): 10.46 (s, NH, 1H), 9.32 (s, NH, 1H), 8.22 (s, 2H), 8.15-7.89 (dd, 4H), 7.62-7.09 (m, 14H), 6.90-6.71 (dd, 4H), 4.13 ppm (s, 2H).^{13}C-NMR (DMSO-d_6): 181.7, 136.9*, 136.3*, 136.2, 135.4*, 135.0*, 130.1*, 128.7*, 128.6, 128.2, 125.2, 122.2, 120.9, 120.4*, 120.1*, 35.4* ppm. ^{29}Si-NMR (DMSO-d_6): −15.2 ppm. Elem. Anal. Calcd. for $C_{39}H_{28}O_2N_2Si$; (584.50): C: 80.14%; H: 4.79%. Found: C: 79.32%; H: 4.01%.

RESULTS AND DISCUSSION

Structure and solubility of the polymers

The FTIR spectra from PEF and PAF polymers showed the disappearance of the band associated to the O—H stretching (COOH group of monomer) and the formation of ester and amide linkage, respectively (1690–1650 cm^{-1} range). This same behavior was observed by Raman analysis. This technique favors the study of vibrations out of plane that are difficult to observe by infrared. Thus, the out of plane C=C vibrations was employed to establish the effect of iodine vapors on the sample. On the other hand, the ^{1}H-NMR spectrum of PAF shows two singlets for amidic NH while the ^{13}C-NMR spectrum shows clearly the aliphatic, aromatic, and carbonyl carbons. The chemical shift of ^{29}Si is similar in both polymers, in agreement with full aromatic environment of silicon atoms.

The solubility of the polymers was tested in various solvents at room temperature. The PEF-2 and PAF-3 polymers were readily soluble in polar protic solvents such as DMF, NMP, DMSO, pyridine, *N,N*-dimethylacetamide, and *m*-cresol, but insoluble in chloroform, dichloromethane, benzene, toluene, ethanol, and methanol. The PEF-12 and PAF-12 polymers were soluble at room temperature in HCl and H_2SO_4 and partially soluble in DMSO.

Optical properties: UV-array diode

Figure 2(a) shows the UV-Vis spectra of the polymer dissolved in DMSO at 25°C. All the polymers, except PAF-3, had the same behavior: two maximum absorption wavelengths in UV-vis region, the first band at 262–293 nm and the second at 315–320 nm (Table I), which is associated to two π-π* bond transitions corresponding to delocalized electrons in the molecule. On the other hand, the PAF-3 polymer showed a high intensity absorption peak at 323 nm, which can be assigned to π-π* transition with an intramolecular charge transfer, related to the polymeric structure and, therefore, to the highest degree of electronic delocalization. Additionally, this compound has an effective mass or number of repetitive units (Table II) higher than the other poly(amide) (PAF-12). This behavior can also be observed for the poly(ester). Thus, PEF-2 showed a higher electron delocalization (resonance) than that of PEF-2.

The band gap energy of polymers was calculated from their adsorption edges using Tauc's extrapolation method.[20] The extrapolation of the straight line portion of the $A(h\nu)^2$ v/s $h\nu$ plot to A=0 for the polymer revealed two optical band gaps for the polymers: the first bands between 4.36-3.39 eV are related to electron delocalization in the aromatic rings of the fluorene moiety. The second band emission at 3.86-3.69 eV might derive from the valence conduction band (π−π*) transition, related to other conjugated segments in the polymers, such as carbonyl groups.

The PEFs and PAFs polymers have a conjugation along the chain, which is an important factor for the charge carrier mobility. However, PEF-2 and PAF-12

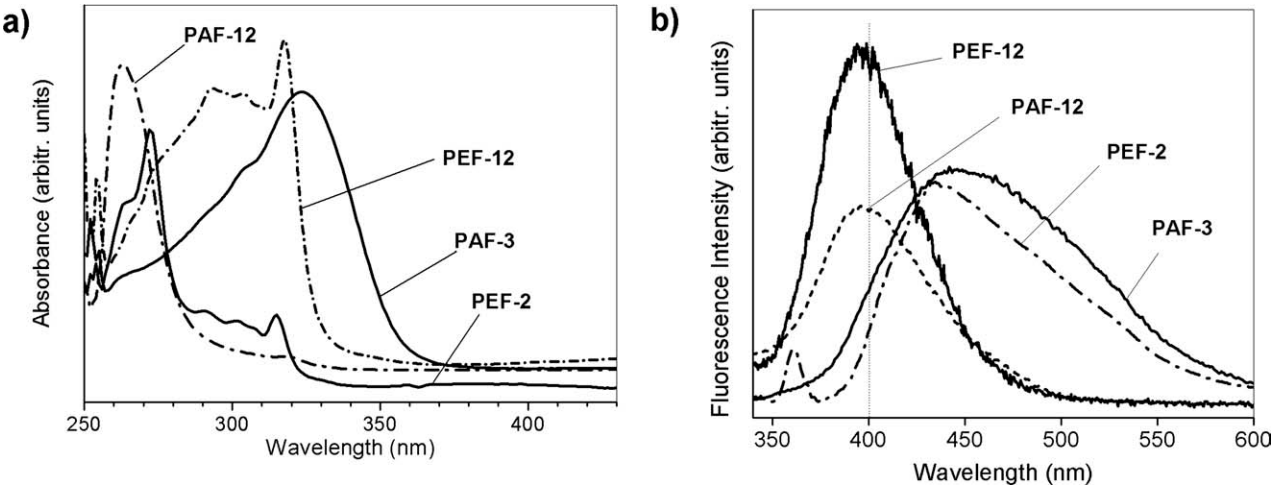

Figure 2 (a) UV-vis absorption spectra and (b) fluorescence emission spectra.

have a higher value of the optical band gap (4.36 eV). This characteristic could be related with a possible torsion between the rings planes, which interrupt the conjugation. The fluorescence measurements were made at wavelengths from 270 to 600 nm at regular intervals with fixed excitation and emission slits at 10 nm. The excitation wavelengths were 327 nm for PEF-2, 315 nm for PEF-12, 320 nm for PAF-3 and 259 nm for PAF-12. The emission spectra of all polymers were independent of the excitation wavelength but strongly dependent on the reaction time. Figure 2(b) shows the fluorescence emission spectra for the polymers, where there is a relation between the reaction time of the polymerization and the emission wavelength: PEF-12 and PAF-12 ($\sim$ 397 nm), PEF-2 and, PAF-3 (435–451 nm). All polymers showed a blue-shifted emission maximum, due to the degree of delocalized π-bond in the system. Thus, the displacement of the emission wavelength is controlled by the conjugation longitude and the reaction time of the polymerization. These observations suggest that the wavelength values increase with the effective mass for poly(amides) (PAF-3) or the possible orientation of the molecules along a common axis for poly(ester) (PEF-2) due to specific interaction between chains. In addition, when the polymeric segments are elongated, there is higher probability for intra as well as intermolecular interactions between the fluorophores, broadening the emission bands. Table I shows the values of absorption band gap and emission sub-band gap. These show values from 2.75 to 3.14 eV, related to light emission of the polymers when the samples were excited to a given wavelength.

TABLE I
UV–Vis Absorption Spectra, Band Gap Absorption, and Sub-Band Gap Emission of the Polymers

Polymers	Absorption (nm)	Band gap absorption (eV)[a]	Sub-band gap emission (eV)[b]
PEF-2	272 and 315	4.36 and 3.86	2.85
PEF-12	293 and 317	3.74	3.14
PAF-3	323	3.39	2.75
PAF-12	262 and 320	4.36 and 3.69	3.12

[a,b] Values taken from Figure 2(a,b), respectively.

Effective mass of the polymers

The effective masses of the polymers were obtained through negative and positive modes. These values were acquired with the Data Analysis 3.2 program (Bruker Daltonik GmbH, Germany) and they correspond to deconvoluted spectra. The wavelengths used were 320 and 326 nm [Fig. 2(a) and Table II].

The studied polymers showed a range of effective mass of 1.59×10^4 to 4.90×10^4 m/z, and 1.22×10^4 to 2.92×19^4 in positive and negative modes, respectively. As expected, the increase of the effective mass is related to the time of polymerization, conjugation of the polymers and, therefore, to their optical properties; they exhibited two tendencies: (1) The polymer with the highest absorption (PAF-3, 323 nm) showed an increase in the effective mass compared with its homologous (PAF-12, 320 nm); (2) The poly(ester) that was polymerized for 12 h

TABLE II
Effective Molecular Mass Obtained by ESI-MASS Spectrometry

Polymers	Effective mass (m/z)	
	Positive polarity	Negative polarity
PEF-2 (320 nm)[a]	1.59×10^4	1.22×10^4
PEF-12 (320 nm)	2.95×10^4	2.92×10^4
PAF-3 (326 nm)	4.90×10^4	2.37×10^4
PAF-12 (320 nm)	3.17×10^4	2.19×10^4

[a] Values of absorption of the polymers taken from Figure 2(a).

TABLE III
Glass Transition, Melting Temperature, and Thermal Decomposition Temperature for the Polymers

	DSC		TDT	
Polymers	T_g [a] (°C)	T_{melt} [b] (°C)	$TDT_{(10\%)}$ [c] (°C)	Residues at 800°C (wt %)
PEF-2	68.6	183.0	340.9	19.9
PEF-12	75.6	n.o.	314.3	39.3
PAF-3	58.2	n.o.	388.5	52.8
PAF-12	50.7	n.o.	216.8	51.2

[a] From the second heating traces of DSC measurements conducted with a heating rate of 20°C min^{-1} in nitrogen atmosphere.
[b] Melting temperature for heating.
[c] Temperature at which a 10% weight loss was recorded by TG at a heating rate of 20°C min^{-1} in nitrogen atmosphere; n.o., not observed.

(PEF-12, 320 nm) showed an increase in the number of repetitive units compared with PEF-3, 320 nm.

Thermal analysis

Table III shows the value of glass transition (T_g) and thermal decomposition temperature obtained for the polymers. Both measurements were realized in nitrogen atmosphere at a heating rate of 20°C min^{-1}. The T_g values were considered as changes in the slope in the DSC curves after second heating run and the thermal stability was examined by TGA measurement (Fig. 3).

Results showed that the PEF-2 and PEF-12 polymers have higher glass transition temperatures than PAF-3 and PAF-12. These higher values are not expected, because the esteroxygen produces an increase in flexibility of the polymer backbone and therefore a decrease of T_g. The only explanation could be related with a reduced packing efficiency and interchain interaction within the polymer.

On the other hand, when the polymerization was carried out for 12 h at the same temperature, PAF-12 polymer showed a decrease of the T_g compared with PAF-3. This behavior could be related to a decreasing rigidity of the polymer backbone, produced by an increase in the reaction time. However, for PEFs the tendency in the T_g values was inverse, without a clear explanation.

The DSC measurements for the PEF-2 polymer showed a melting peak at 183°C (Table III), associated to a crystalline morphology, which was ratified by X-ray diffraction analysis.

Figure 3 shows the TGA (25–900°C) traces for PEFs and PAFs. The PEFs have a lower thermal stability than the PAFs polymers, showing a decomposition temperature of around 430°C, which corresponds to the decomposition of the ester group. At this temperature, PAF-12 shows a considerable weight loss (~ 75% mass loss) that could be related with the preferential structural arrangement, with an increase in the flexibility of the polymer. The higher thermal stability of the PAFs could be a consequence of the amide linkage, which confers structural rigidity, in part due to the hydrogen bonding abilities of amides. The weight residues at 800°C for the polymers were 19–52%, which reveals that these polymers lose weight due to degradation of the polymer chain itself (Table III).

X-ray diffraction

The structures of the polymers were investigated by X-ray diffraction at room temperature. PEF-2 produced several sharp diffraction peaks [Fig. 4(a)], indicating a crystalline structure. Several structures, such as trigonal, monoclinic, and hexagonal, were employed to try to fit with these diffraction peaks.

The best fit was found for a monoclinic packing, which has the following lattice parameters: $a = 5.42$ Å, $b = 6.90$ Å, and $c = 11.32$ Å with angles $\beta = 75.30°$ and $\alpha = \gamma = 90°$. For this, we define a monoclinic structure with primitive vectors:

$$\vec{a} = a\hat{x}$$
$$\vec{b} = b\hat{y}$$
$$\vec{c} = c\cos\beta\hat{x} + c\sin\beta\hat{z}$$

where a, b, c are the lattice parameters of the monoclinic structure. Then we generate the following $d(h, k, l)$ spacing for Miller indexes (h, k, l).

$$d(h,k,l) = \frac{1}{\sqrt{\frac{h^2}{a^2} + \frac{k^2}{b^2} + \left(\frac{l}{c\sin\beta} - \frac{\cos\beta}{\sin\beta}\frac{h}{a}\right)^2}}$$

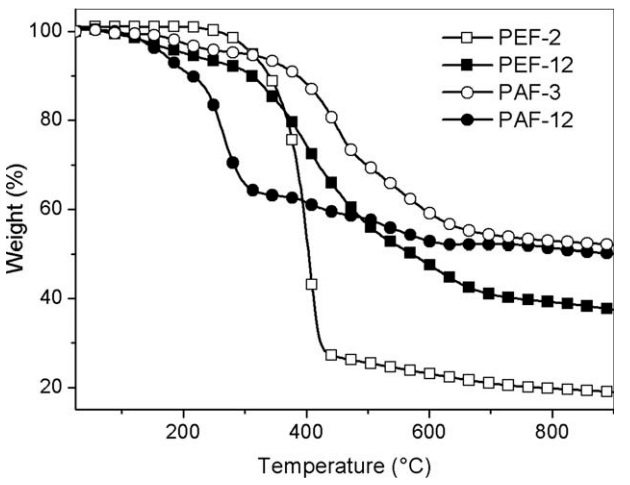

Figure 3 TGA curves for the polymers; PEF-2, PEF-12, PAF-3, and PAF-12 at a heating rate of 20°C min^{-1}.

The experimental $d(h, k, l)$ spacing we obtained from the Bragg formula using the diffraction data is:

$$d(h,k,l) = \frac{\lambda}{2\sin\theta}$$

The fitting is obtained from a refinement calculation with trials for different values of h, k, l, a, b, and c parameters and β angle until all the experimental and theoretical $d(h, k, l)$ spacing coincides with an error better than 0.05 Å for all the peaks.

Using the monoclinic lattice obtained we were able to generate crystals planes that diffracted X-rays in all of the 2θ angles shown in Figure 4(a). An estimated value of the extended molecule of the repetitive unit of PEF (shown in Fig. 1) is 19.71 Å. This value is larger than the c parameter of the monoclinic structure; thus we suspect that a pitch in the molecule is present at the ester group.

On the other hand, PEF-12 and PAF-12 [Fig. 4(b)] showed amorphous patterns. These results could be explained by the reduction of the rigidity of the polymer chains, associated with an increase in the reaction time, due to the movement acquired by the polymer main chains in solution, producing cross-linking between them.

Raman spectroscopy

The Raman spectroscopy of the polymers with and without exposure to iodine vapor, showed an equal contribution of vibrations. The only difference between PAF-3 and PAF-12 is related with the C=C stretching and out-of-plane deformation of aromatic rings, which reveals that there is less regioregularity into the structure of the polymer [Fig. 5(a)]. Specifically, the band at $\sim$ 934 cm^{-1} corresponds to the absorption of the C=C bending mode, which appears as a consequence of doping. This new band may be due to a radical cation species, which is formed upon charge-transfer.[29] Additionally, the increase in rigidity of the polymeric chains upon doping, may be caused by an interchain cross-linking process mediated by the radical species that are generated.

PAFs (without doping), Raman (cm^{-1}): 1614 (C=O stretching), 1596 (Si—C arom.); 1485 (C—N stretching and N—H bending), 1520 (C=C arom. stretching), 1412 (CH_2 deformation); 1321, 1284 (CH_2 wag), 1189 (C=C in plane arom. bending), 996 (C=C arom. *oop* deformation).

PAFs (with doping), Raman (cm^{-1}): 1613 (C=O stretching), 1595 (Si—C arom.), 1482 (C—N stretching and N—H bending); 1413 (CH_2 deformation), 1324, 1282 (CH_2 wag), 1188 (C=C arom. *oop* bending), 996-934 (C=C arom. *oop* deformation).

PEFs without exposure to iodine vapor showed a spectrum with a broad fluorescence band [Fig. 2(b)] without any obvious Raman peaks, except the band at 1614 cm^{-1}, which is assigned to C=O stretching of the aromatic rings [Fig. 5(b)]. When the polymer is doped with iodine the fluorescence decreases due to a conformational change, which is observed in Raman spectra. Thus, the polymer loses flexibility upon doping, showing different vibrations.

PEFs (without doping) Raman (cm^{-1}): 1614 (C=O stretching). PEFs (with doping) Raman (cm^{-1}): 1611

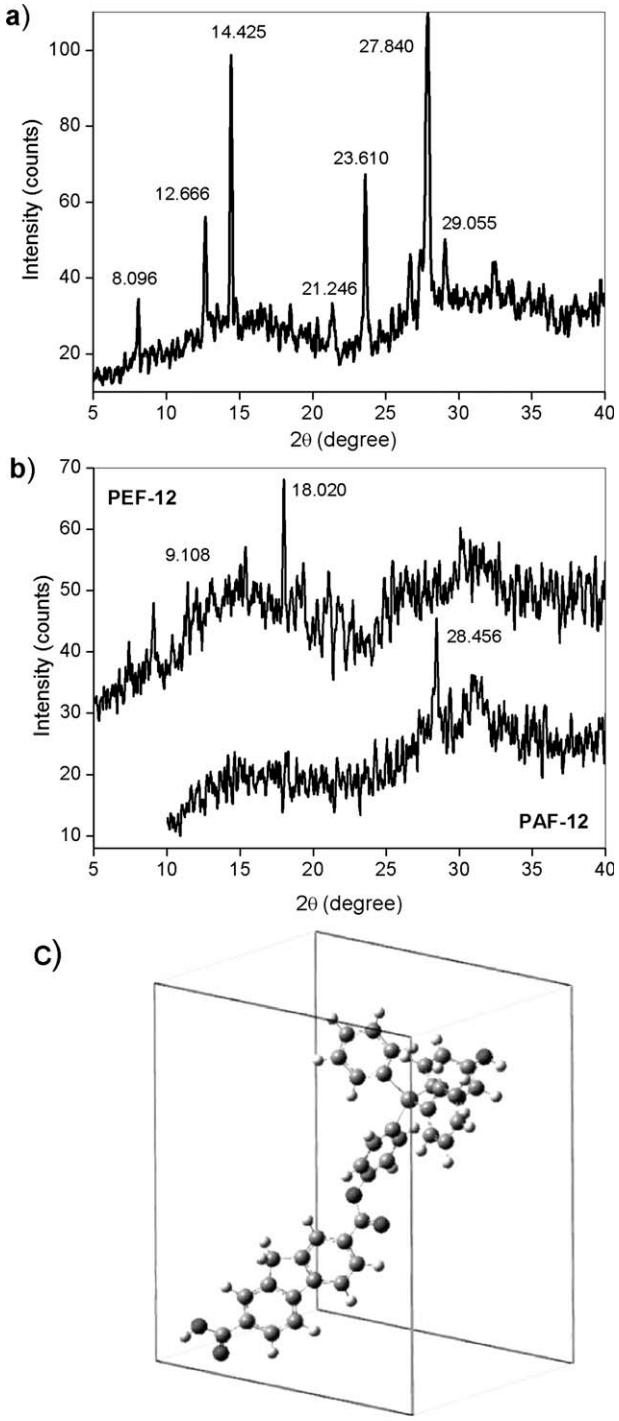

Figure 4 X-ray diffractograms: (a) PEF-2; (b) PEF-12; PAF-12; and (c) Monoclinic packing of PEF-2.

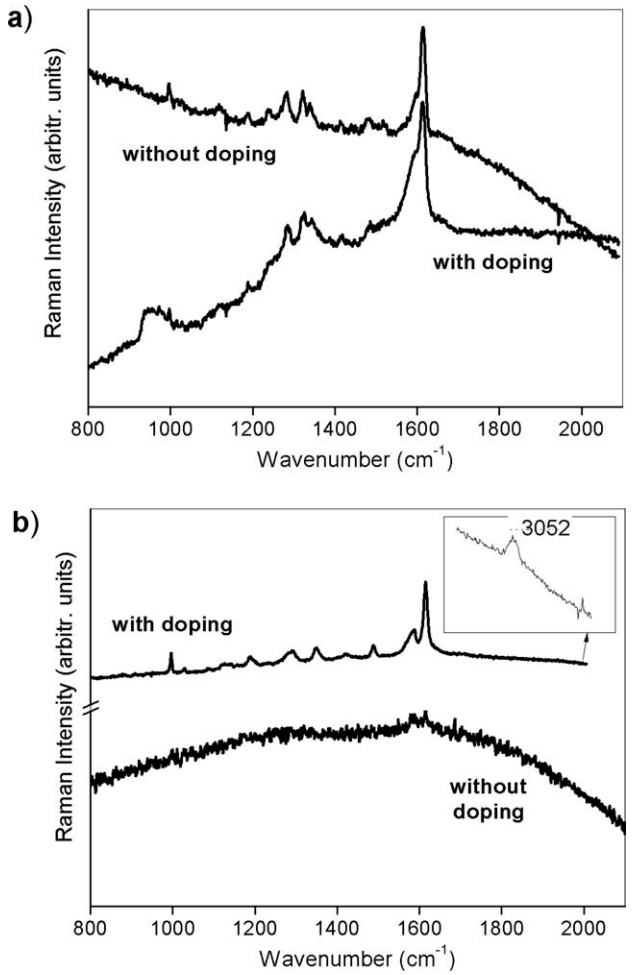

Figure 5 FT Raman spectra of thin films with doping and without doping: (a) PAFs, (b) PEFs.

(C=O stretching), 1586 (Si—C arom.), 1485 (CH_2 deformation), 1345, 1288 (CH_2 wag), 1190 (C(O)—O stretching), 997 (C=C arom. *oop* deformation), 779 (CH_2 rock).

Conductivity

The polymers were deposited on a silicon substrate (SiO_2/Si(100)) of 1 cm^2 area from the DMSO solution and dispersed at 1000 rpm for 45 s by spin coating. The polymer coated substrates were annealed at 80°C for 12 h in vacuum for the elimination of the occluded solvent.

The thickness of the film was determined with a custom-made ellipsometer in a single wavelength null-PCSA configuration with a fixed angle of incidence.[30] For thick films the polarizer and analyzer angles were determined. The film thickness was calculated solving the complete Drude equations using a FORTRAN routine.[31] For calculations we assumed for the undoped polymer films a refractive index between $n = 1.45$ and 1.55. The values for the average film thickness and the errors resulting from the assumed minima and maxima refractive indices are shown in Table IV.

The conductivity was measured on polymeric films before and after exposure to iodine vapors, using a four point probe connected to a digital multimeter. The results obtained with this technique are at surface level; therefore, the values are strongly affected by the order of the molecules and the macroscopic homogeneity of the film. The sample is exposed to iodine vapor for three days until constant weight[32,33] in order to generate charge carriers into the polymeric system.

The conductivity was measured before and after introduction of carrier doping. Before oxidation the conductivity was between 2.15 and 4.63 $\times$ 10^{-5} S cm^{-1}. In general, these values decrease after the doping (Table IV), which could be related with a certain degree of disorder of the molecules within the system, showing a clear relation between surface morphology, homogeneity, film thickness, and conductivity.

Our results suggest that the small increase of electrical conductivity of PEF-12 and PAF-3 in comparison to PEF-2 and PAF-12, respectively, before of the oxidation, is associated with a slight decrease of the optical band gap (Table I). This fact is a consequence of an increased density of localized states in the gap due to the possible deformation of the partially crystalline structure, which presents a certain degree of order by the folding and stacking of the chains [Fig. 4(b)]. Thus, the increase of the disorder degree promotes the appearance of band tails in the spectrum, which is accordance with the electronic structure of amorphous materials.

The polymers after the doping process exhibited conductivity in the range 1.30 to 1.90 $\times$ 10^{-5} S cm^{-1}. These values are higher than the conductivities shown by the natural polymer system (10^{-12} and 10^{-16} S cm^{-1}).[34] According with the results obtained, it is possible to suggest that is necessary a totally conjugated backbone for the generation of conducting polymers. This fact would allow a partial charge in the aromatic ring and, therefore, an electron

TABLE IV
Conductivity of the Polymers with and Without Doping to Different Thickness of the Film

Polymer	Thickness of the film (Å)	Apparent conductivity (1×10^{-5} S cm^{-1}) Undoped	Doped
PEF–2	2744 (±) 250	2.15	1.30
PEF–12	2805 (±) 250	3.30	1.44
PAF–3	2763 (±) 250	4.63	1.54
PAF-12	2676 (±) 250	2.38	1.90
PAF–12	5877 (±) 250	1.90	7.70

delocalization in the system. Exceptionally, a slight increase in the conductivity after doping was observed for the PAF-12 polymer with a thickness of 5877 (±) 250 Å (Table IV). This behavior could be related with an increase of ordered regions (regioregularity), structural homogeneity, crystallinity and/or film thickness.

On the other hand, this behavior has also been widely studied in polymers such as poly(heterocyclic)s, based on poly(thiophene)[35] and poly(pyrrole).[36] Changes in the morphology of these systems were related to the removal of one electron caused by introduction of charge species, using iodine vapors. Similar results were shown by poly(aniline),[37–39] which seem to be the most interesting conducting polymer.

It is known to halogen doping can be used to produce structural change in some polymers. Thus, Nylon is an example of poly(amide)s in which the iodination produces significant structural changes.[40,41] Under certain experimental condition, Nylon 6-iodine complexes are considered good solid-state electrolytes than can be used as electrode material showing very high conductivity.[42]

Moreover, the study of the physical properties, conductivity, and structural change during iodine desorption of poly(ester)s and poly(amides)s with fluorene and diphenyl-silane units in the main chain (Fig. 1) has not been carried out previous to this work.

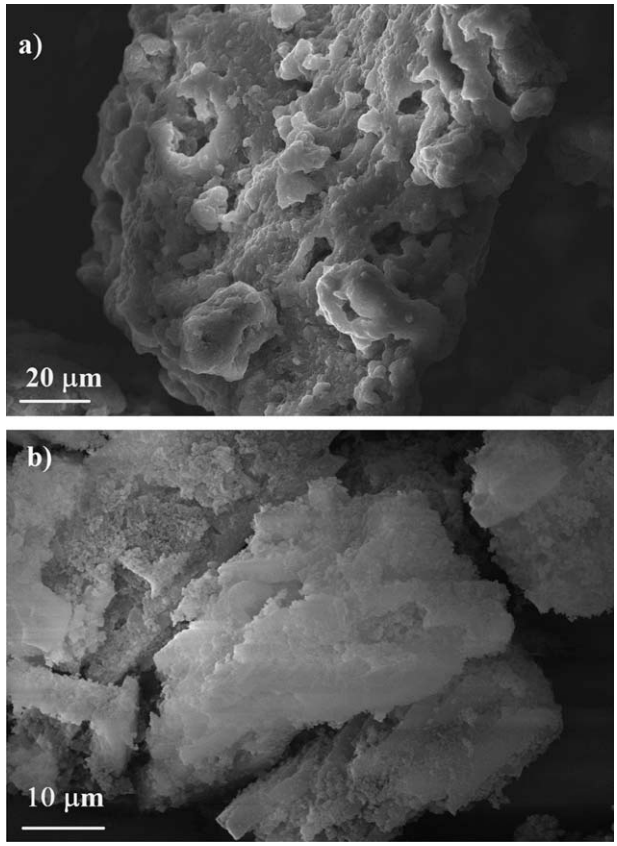

Figure 6 SEM micrographs of the polymers: (a) PAF and (b) PEF.

Scanning electronic microscopy

SEM of the polymers before oxidation in solid phase

Figure 6(a) shows the electron micrograph of the polymers, where PAFs exhibits a different surface with great porosity. For this reason, when this polymer is exposed to iodine vapor, it has the capacity to absorb this molecule like a sponge, producing an oxidation of the material and, therefore, a variation in the conductivity. Additionally, the absorption of iodine is also related to the presence of nitrogen atoms (amidic groups) in the polymer backbone and to the formation of the stable complex [iodine-poly(amide)], due to the lone pair on nitrogen atom sp^2 orbital, which has an impact on the electronic structure (Table IV, PAF-12 thickness= 5877 (±) 250 Å). On the other hand, PEFs show a laminar morphology with a major grade of order and compaction, thereby reducing the oxidation of the polymer [Fig. 6(b)]. On the other hand, when the poly(ester) is exposed to iodine vapors, the electronegativity of the oxygen atoms from the ester groups disfavors the formation of the complex and, therefore, the oxidation of the material. To understand the mechanism of crystal packing and/or lamellar characteristics is necessary to explain the procedure of the polymer crystallization. When the reaction is finished (2 h at 120°C), the polymer is stabilized at room temperature, producing spherulites in solution, which are associated with nucleation sites and, consequently, to ordered lamellae. However, the morphology adopted by the polymers and, therefore, their densities are not related to the substantial increase in the electrical conductivity. This fact would be due to the poor removal of hydrogen atoms by action of the oxidant agent, possibly caused by the lack of diffusion of iodine into the polymer, associated to the higher mass of counterion formed by the vapors (I_3^- and I_5^-). It is known that iodine vapors increase the conductivity over eight orders of magnitude in conjugated polymers ($R\text{-}(CH)_X$), producing charge transfer complexes between the polymer and halogen (acting as a counter anion).[43]

SEM and energy dispersive x-ray analysis of the oxidized polymers

The slight change of conductivity between polymers with and without doping is shown in Table IV. This behavior is probably due to the small modification of the polymeric structure, when the incorporation of charged species within the system is produced. Some factors that could affect the electrical conductivity are related to the conjugation in the polymeric chain (delocalization of charge through the aromatic

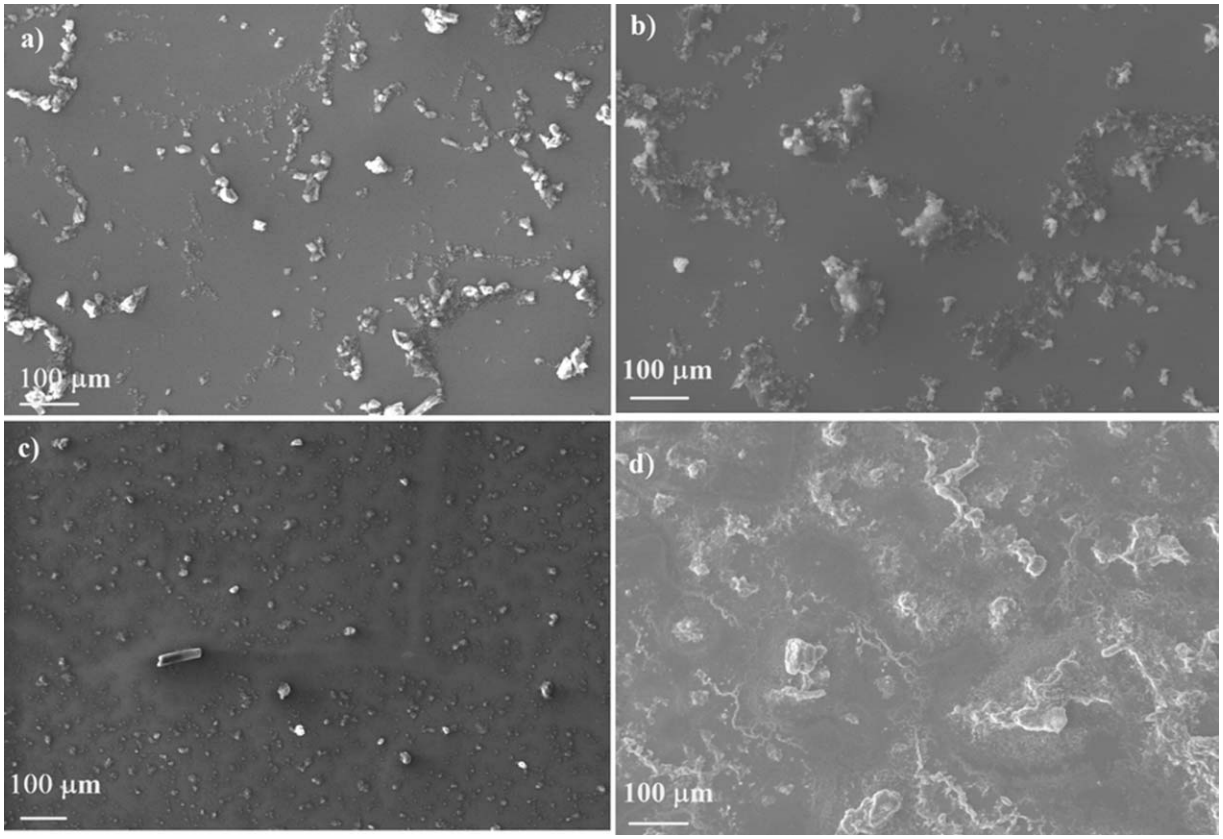

Figure 7 Scanning electron micrographs of polymer films with doping on a silicon wafer: (a) PEF-2; (b) PEF-12; (c) PAF-3; and (d) PAF-12 (5877 (±) 250 Å).

ring, resonance) and also steric hindrance. However, in our case the conjugation of the polymers is interrupted by the ester and amidic group and the conformation that can adopt the polymeric chain in the system.

The granules in the micrographs [Fig. 7(a,b,c)] indicate the formation of micro-domains like islands over the polymeric surface when the oxidation with iodine vapors is produced. The molecules of iodine have the ability to induce stress on the polymer, due to their high molecular size, producing a break in the symmetry of the system and, therefore, heterogeneity of the film. Thus, the loss of conductivity is related to the structural conformation change of the polymeric chains.

Typically, the mechanism of conduction observed in these films is related to the density of charge produced by the iodine vapors. Therefore, homogenous films could increase the probability of charge transport in the system. [Fig. 7(d)] and increase the value of conductivity.

On the other hand, EDX analysis (Fig. 8) corroborates the presence of iodine in the PAF-3 polymers, showing a decrease in the carbon and oxygen region. Additionally, the increase of silicon is related to the substrate (SiO_2/Si), which was used to deposit the polymer.

CONCLUSIONS

All the polymers were successfully prepared by the direct polycondensation of the monomers. Diacid (**3**) and bisphenol (**4a**) was polymerized using thionyl chloride/DMF/pyridine as condensing agent to prepare a new poly(ester) (PEF), and the reaction of diacid (**3**) and diamine (**4b**), using TPP and pyridine,

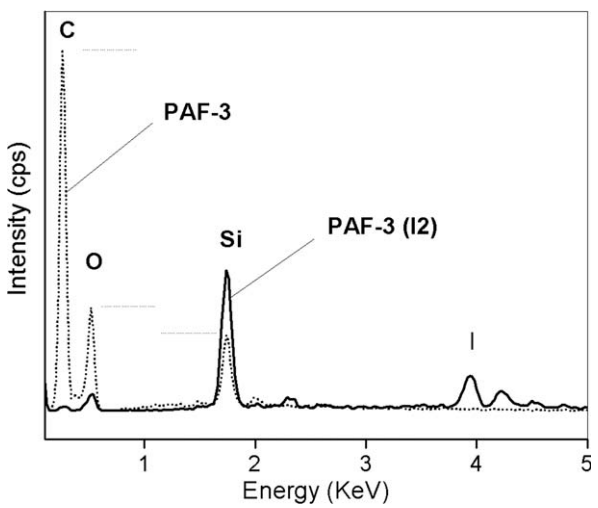

Figure 8 EDX spectra for the polymer PAF-3, doped (I2) and undoped.

as condensing agent to prepare poly(amide) (PAF). The influence of the reaction time on the physical and electrical properties of the resulting polymer was studied. Polymers were characterized by spectroscopy methods and the results were in agreement with the proposed structures. These compounds are soluble in various organic solvents (polar aprotic solvents) and have moderate thermal stability. The incorporation of amide group in the polymer reduces the glass transition temperature based on free surface effect. The time and temperature of crystallization is related with the morphology that adopts the polymeric chain (crystalline and amorphous regions). The values of sub-band gap states related to the emission of the light are lower than that obtained by band gap absorption. This behavior is related to the amount of chromophores in the system. In fact, the polymers that presented higher electron delocalization also showed a higher effective mass or the possible orientation of the molecules along a common axis, due to intra or intermolecular interactions. On the other hand, the increase of thickness of the sample, resulted in conductivities slightly higher. This fact would be associated to an improvement in the macroscopic homogeneity of the film, and therefore, to a higher distribution of charge density. Thus, the conductivity is related to the density of charges produced by the iodine vapors; therefore, in homogenous films of significant thickness, the probability of charge transport in the system increases. EDX analysis showed a regular distribution of iodine in the polymer and a decrease of carbon and oxygen region in the system.

Thanks are due to M. Soto, M. Pino, and R. Trabol for SEM, XRD, and conductivity characterization.

References

1. Miller, R. D.; Wilson, C. G.; Wallraff, G. M.; Clecak, N.; Sooriyakumaran, R.; Michl, R.; Karatsu, J.; McKinley, A. J.; Klingensmith, A. J.; Downing, J. Polym Eng Sci 1989, 29, 882.
2. Blazsó, M.; West, R.; Székely, T. J Anal Appl Pyrolysis 1989, 15, 175.
3. Wolff, R.; West, R. Appl Organomet Chem 1987, 1, 7.
4. Kepler, R. G.; Zeigler, J. M.; Harrah, L. A.; Kurtz, S. R. Phys Rev B 1987, 35, 2818.
5. Fujino, M. Chem Phys Lett 1987, 136, 451.
6. Marinero, E. E. Chem Phys Lett 1985, 115, 501.
7. Kajzar, F.; Messier, J.; Rosilio, C. J Appl Phys 1986, 60, 3040.
8. Baumert, J. C.; Bjorklund, G. C.; Jundt, D. H.; Jurich, M. C.; Looser, H.; Miller, R. D.; Rabolt, J.; Soorijakumaran, R.; Swalen, J. D.; Twig, R. J. J Appl Phys Lett 1988, 53, 1147.
9. Matsumoyo, N. Kotai Butsuri 1987, 22, 907.
10. Tagle, L. H.; Díaz, F. R.; Vega, J. C.; Valenzuela, P. Eur Polym J 2003, 39, 407.
11. Tagle, L. H.; Díaz, F. R.; Vega, J. C.; Quezada, M.; Guerrero, P. J Inorg Organomet Polym 2003, 13, 21.
12. Terraza, C. A.; Tagle, L. H.; Leiva, A.; Vega, J. C. Polym Bull 2004, 52, 101.
13. Tagle, L. H.; Terraza, C. A.; Valenzuela, P.; Leiva, A.; Urzúa, M. Thermochim Acta 2005, 425, 115.
14. Tagle, L. H.; Terraza, C. A.; Alvarez, P.; Vega, J. C. J Macromol Sci Part A: Pure Appl Chem 2005, 42, 301.
15. Terraza, C. A.; Tagle, L. H.; Leiva, A. Polym Bull 2005, 55, 277.
16. Tagle, L. H.; Terraza, C. A.; Alvarez, P. Phosphorus Sulfur Silicon Related Elements 2006, 181, 239.
17. Terraza, C. A.; Tagle L. H.; Leiva, A.; Poblete, L.; Concha, F. J. J Appl Polym Sci 2008, 109, 303.
18. Tagle, L. H.; Terraza, C. A.; Leiva, A.; Devilat, F. J Appl Polym Sci 2008, 110, 2424.
19. Bøggild, P.; Grey, F.; Hassenkam, T.; Greve, D. R.; Bjørnholm, T. Adv Mater 2000, 12, 947.
20. Tauc, J.; Grigorovici, R.; Vancu, A. Physica Status Solidi (b) Basic Res 1966, 15, 627.
21. Friedman, L.; Shechter, H. J Org Chem 1961, 26, 2522.
22. Davidsohn, W.; Laliberte, B. R.; Goddard, C. M.; Henry, M. C. J Organometal Chem 1972, 36, 283.
23. Gilman, H.; Beel, J. A.; Brannen, C. G.; Bullock, M. W.; Dunn, G. E.; Miller, J. S. J Am Chem Soc 1949, 71, 1499.
24. Pratt, J. R.; Thames, S. F. J Org Chem 1973, 38, 4271.
25. Mallakpour, S.; Shahmohammadi, M. H. Iranian Polym J 2005, 14, 974.
26. Mallakpour, S.; Kowsari, E. J Appl Polym Sci 2006, 101, 455.
27. Mallakpour, S.; Kowsari, E. Polym Bull 2005, 55, 51.
28. Hsiao, S.-H.; Yang, C.-P.; Chu, K.-Y. J Polym Sci A Polym Chem 1997, 35, 1469.
29. Thakur, M. Macromolecules 1998, 21, 661.
30. Volkmann, U. G.; Pino, M.; Altamirano, L. A.; Taub, H.; Hansen, F. Y. J Chem Phys 2002, 16, 2107.
31. Cisternas, E. A.; Corrales, T. P.; Campo, V.; Soza, P. A.; Volkmann, U. G.; Bai, M.; Taub, H.; Hansen, F. Y. J Chem Phys 2009, 131, 114705.1.
32. Kowalik, J.; Tolbert, L. M.; Narayan, S.; Abhiraman, A. S. Macromolecules 2001, 34, 5471.
33. Chiang, C. K.; Fincher, C. R.; Park, Y. W.; Heeger, A. J.; Shirakawa, H.; Louis, E. J.; Gau, S. C.; MacDiarmid, A. G. Phys Rev Lett 1977, 39, 1098.
34. Shirakawa, H.; Louis, E. J.; MacDiarmid, A. G.; Chiang, C. K.; Heeger, A. J. J Chem Soc Chem Comm 1977, 16, 578.
35. Zhang, D. Y.; Porter, T. L. Synth Met 1995, 74, 55.
36. Yagüe, J. L.; Agulló, N.; Borrós, S. Plasma Proc Polym 2008, 5, 433.
37. Wang, L.; Jing, X.; Wang, F. Synth Met 1991, 41, 739.
38. Gizdavic-Nikolaidis, M.; Graham, A.; Bowmaker, G. Polymer 2008, 49, 3070.
39. Sarkar, A.; Ghosh, P.; Meikap, A. K.; Chattopadhyay, S. K.; Chatterjee, S. K.; Chowdhury, P.; Roy, K.; Saha, B. J Appl Polym Sci 2008, 108, 2312.
40. Shabana, H. M. J Phys D: Appl Phys 2006, 39, 2843.
41. Abu-Isa, I. J Polym Sci Part A-1 1971, 9, 199.
42. Yamamoto, T.; Kuroda, S. J Electroanal Chem 1983, 158, 1.
43. Hall, J. W.; Arbuckle, G. A. Macromolecules 1996, 29, 546.